Wireless power transfer for a pacemaker application

Vladimir Vulfin[a], Shai Sayfan-Altman[b] and Reuven Ianconescu[c]

[a]Department of Electrical and Computer Engineering, Ben-Gurion University of the Negev, Beer Sheva 84105, Israel; [b]ANSYS inc. 26 Harokmim St., Holon, Israel; [c]Shenkar College of Engineering and Design 12, Anna Frank St., Ramat Gan, Israel

ARTICLE HISTORY
Compiled August 11, 2018

ABSTRACT
An artificial pacemaker is a small medical device that uses electrical impulses, delivered by electrodes contracting the heart muscles, to regulate the beating of the heart. The pacemaker is implanted under the skin, and uses for many years regular non rechargeable batteries. However, the demand for rechargeable batteries in pacemakers increased, and the aim of this work is to design an efficient charging system for pacemakers.

KEYWORDS
pacemaker; wireless power transfer; mutual inductance

1. Introduction

Pacemakers are in use since 1958, and the first implanted pacemakers where based on rechargeable Nickel-cadmium batteries [1]. These pacemakers were recharged by holding an inductive coil up against the skin, near the pacemaker, for several hours. This procedure had to be repeated every few days. Rechargeable pacemakers at this time have been abandoned for two reasons. First, Nickel-cadmium batteries have a relatively short service life, so in spite of being rechargeable, those pacemakers still needed to be replaced often. Second, patients often forgot to recharge their pacemakers according to the recommended schedule [2].

Because of the advance in technology, and the development of longer lasting non rechargeable batteries, the pacemakers based on rechargeable batteries have been abandoned. The new mercury-zinc batteries that have been developed at this time could keep a pacemaker going for up to two years. In 1973 lithium-iodide batteries were developed, which could power a pacemaker for an even longer period of about 5 to 10 years. It is to be mentioned that even longer lasting batteries, based on plutonium have been developed [1], but those have been abandoned due to the toxicity of plutonium, so most pacemakers today need to be replaced after a typical period of around 10 years.

Currently, there is a new interest in developing rechargeable pacemakers [3–7] which could improve the quality of life of the patients. The current paper develops a recharge system for pacemakers at a low frequency of 20kHz. The efficiency is lower at low

CONTACT Reuven Ianconescu Email: riancon@gmail.com

frequency, but also the eddy currents are smaller, making it easier to comply with EMF safety standards limits [5, 8–10]. It is worth to mention that there is a two fold increase in eddy currents at high frequencies: the electric field is proportional to the frequency, and the human body conductivity increases with the frequency, hence the advantage of the low frequency. To overcome the low efficiency problem we use a ferrite core and an aluminium plate for increasing the coupling between the primary and secondary coils, which proves effective.

In section 2 we give a short theoretical background on transformers, mutual inductance, and coupling. We also show how to derive the equivalent circuit of the transformer. In section 3 we discuss the eddy losses and how they affect the equivalent circuit. In section 4 we explain the system that we developed using ANSYS "Maxwell" and "Simplorer" tools, and analyse its performances. The work is ended with some concluding remarks.

2. Mutual inductance and coupling coefficient

The key to achieve a good power transfer between the primary and secondary coils is to obtain a good coupling between them. A perfect coupling is obtained if the flux lines of both coils overlap, and in air, this can only happen if the coils themselves overlap.

To explain this principle we look at a regular transformer built on a magnetic material core, shown in Figure 1. The magnetic material, having a high magnetic

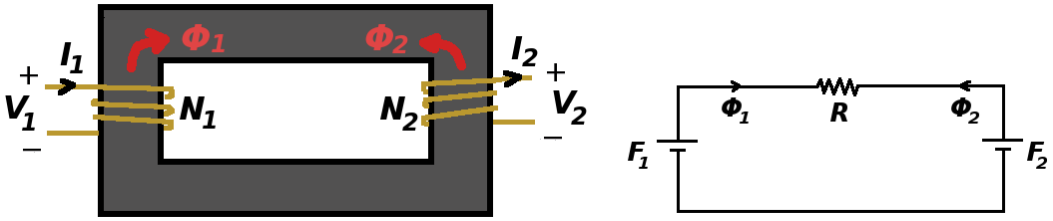

Figure 1. The left diagram shows a transformer built on a magnetic core, while the right diagram shows the electric analogue to the transformer magnetic circuit. The primary and secondary have $N_{1,2}$ turns respectively and their currents are defined as $I_{1,2}$, so that their direction indicates AC power entering into the primary and exiting from the secondary, according to the definition of the induced voltages $V_{1,2}$, which are referred further on. The magneto-motive forces of the primary and secondary are $\mathcal{F}_{1,2} = N_{1,2}I_{1,2}$ respectively, and the fluxes $\Phi_{1,2}$ are defined according to the polarity of magneto-motive forces. The magnetic reluctance of the core is $\mathcal{R}$.

permeability, i.e. a low magnetic reluctance, "guides" the flux lines so that they close through the core. Hence, if one either feeds the primary, leaving the secondary open, or vice-versa, the flux lines have the same trajectories, i.e. the coupling is perfect. We call the magnetic reluctance of the core $\mathcal{R}$ and define the primary current I_1 as "entering", while the secondary as "exiting", anticipating the power to enter into the primary and exit from the secondary. The fluxes are called Φ_1 and Φ_2 are defined in opposite directions (to match the definitions of the currents I_1 and I_2) so that $\Phi_1 = -\Phi_2$.

For this magnetic circuit we define the primary and secondary magneto-motive forces $\mathcal{F}_1 = N_1 I_1$ and $\mathcal{F}_2 = N_2 I_2$, expressing:

$$\Phi_1 = -\Phi_2 = \frac{\mathcal{F}_1 - \mathcal{F}_2}{\mathcal{R}} \tag{1}$$

Using the 2 port network definition for the induction matrix

$$\begin{pmatrix} N_1\Phi_1 \\ N_2\Phi_2 \end{pmatrix} = \begin{pmatrix} L_1 & -M_{12} \\ -M_{21} & L_2 \end{pmatrix} \begin{pmatrix} I_1 \\ I_2 \end{pmatrix}, \tag{2}$$

We define the primary and secondary inductances

$$L_1 = \left.\frac{N_1\Phi_1}{I_1}\right|_{I_2=0} ; L_2 = \left.\frac{N_2\Phi_2}{I_2}\right|_{I_1=0} ; M_{12} = -\left.\frac{N_1\Phi_1}{I_2}\right|_{I_1=0} ; M_{21} = -\left.\frac{N_2\Phi_2}{I_1}\right|_{I_2=0} \tag{3}$$

Because of reciprocity $M_{21} = M_{12}$, hence we call it M. We define the coupling coefficient

$$k = \frac{M}{\sqrt{L_1 L_2}} \tag{4}$$

which may have values between 0 (no coupling) and 1 (perfect coupling).

Using Eq. (1) one obtains

$$L_1 = \frac{N_1^2}{\mathcal{R}} \quad ; \quad L_2 = \frac{N_2^2}{\mathcal{R}} \quad ; \quad M = \frac{N_1 N_2}{\mathcal{R}}, \tag{5}$$

so that $k = 1$, meaning a perfect coupling, because both primary and secondary have the same flux trajectories. In the case of perfect coupling the induced voltages into primary and secondary satisfy the relation $V_1/V_2 = N_1/N_2$.

A non perfect coupling, which can be solved analytically is shown in Figure 2. The

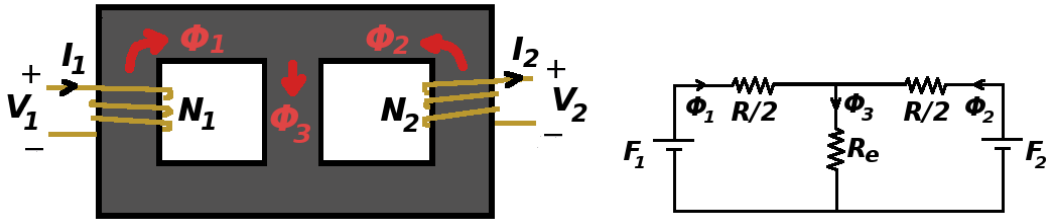

Figure 2. Same as Figure 1, except of the existence of an additional branch in the magnetic core, which we call the "escape" branch. The magnetic reluctance of the original core is now divided between the left and right branch, each one having the reluctance $\mathcal{R}/2$. The flux in the "escape" branch is Φ_3 and its reluctance is $\mathcal{R}_e$.

middle branch represents a "flux escape" branch and has the magnetic reluctance $\mathcal{R}_e$. Solving the magnetic circuit results in Φ_1, Φ_2 and $\Phi_3 = \Phi_1 + \Phi_2$:

$$\Phi_1 = \frac{\mathcal{F}_1 - \mathcal{F}_2}{\mathcal{R}} + \frac{\mathcal{F}_1 + \mathcal{F}_2}{4\mathcal{R}_e + \mathcal{R}} \; ; \; \Phi_2 = \frac{\mathcal{F}_2 - \mathcal{F}_1}{\mathcal{R}} + \frac{\mathcal{F}_1 + \mathcal{F}_2}{4\mathcal{R}_e + \mathcal{R}} \; ; \; \Phi_3 = 2\frac{\mathcal{F}_1 + \mathcal{F}_2}{4\mathcal{R}_e + \mathcal{R}}. \tag{6}$$

Using Eqs. (3) we obtain

$$L_1 = \left(\frac{N_1^2}{\mathcal{R}} + \frac{N_1^2}{4\mathcal{R}_e + \mathcal{R}}\right) ; L_2 = \left(\frac{N_2^2}{\mathcal{R}} + \frac{N_2^2}{4\mathcal{R}_e + \mathcal{R}}\right) ; M = \left(\frac{N_1 N_2}{\mathcal{R}} - \frac{N_1 N_2}{4\mathcal{R}_e + \mathcal{R}}\right). \tag{7}$$

The coupling coefficient is

$$k = \frac{1/\mathcal{R} - 1/(4\mathcal{R}_e + \mathcal{R})}{1/\mathcal{R} + 1/(4\mathcal{R}_e + \mathcal{R})} = \frac{\mathcal{R}_e}{\mathcal{R}_e + \mathcal{R}/2}. \tag{8}$$

If $\mathcal{R}_e \to \infty$, no flux through the "escape branch", and we return to the previous case $k = 1$, and if $\mathcal{R}_e \to 0$ the connection between primary and secondary is lost, so that $k = 0$. The result for k in Eq. (8) represents a flux divider in Figure 2:

$$k = \left.\frac{-\Phi_2}{\Phi_1}\right|_{\mathcal{F}_2=0}, \tag{9}$$

i.e. which part of the primary flux reaches the secondary, when only the primary is fed.

Finally, the primary and secondary voltages are expressed by

$$\begin{pmatrix} V_1 \\ V_2 \end{pmatrix} = \frac{d}{dt}\begin{pmatrix} N_1\Phi_1 \\ -N_2\Phi_2 \end{pmatrix} = j\omega \begin{pmatrix} N_1\Phi_1 \\ -N_2\Phi_2 \end{pmatrix}, \tag{10}$$

where the minus is due to the polarities of Φ_2 and V_2 in Figures 1 and 2. Using Eq. (2) one gets

$$\begin{pmatrix} V_1 \\ V_2 \end{pmatrix} = \begin{pmatrix} j\omega L_1 & -j\omega M \\ j\omega M & -j\omega L_2 \end{pmatrix}\begin{pmatrix} I_1 \\ I_2 \end{pmatrix} = \begin{pmatrix} j\omega L_1 & j\omega M \\ j\omega M & j\omega L_2 \end{pmatrix}\begin{pmatrix} I_1 \\ I_2' \end{pmatrix}, \tag{11}$$

where we defined $I_2' = -I_2$, to have both currents "entering", as usually defined for impedance matrices. This defines the equivalent circuit in Figure 3. It is to be

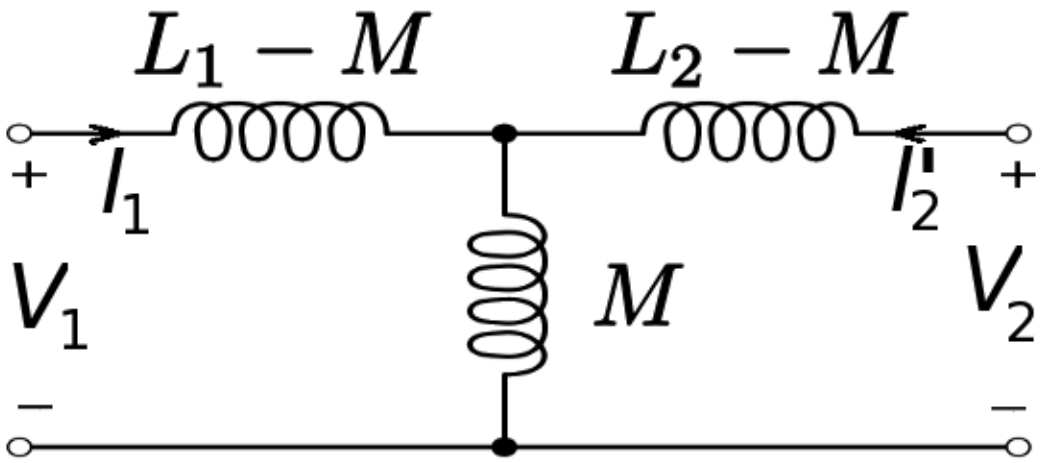

Figure 3. Equivalent circuit describing Eq. (11).

mentioned that one of the inductances $L_1 - M$ or $L_2 - M$ may be negative in case of strong coupling. Those negative values may be avoided by reflecting everything to the primary side of the transformer, i.e. by scaling the output voltage by the factor $N_1/N_2 = \sqrt{L_1/L_2}$, and by scaling the output current by $N_2/N_1 = \sqrt{L_2/L_1}$. We shall leave it as is, because the ANSYS computation tool "Maxwell" calculates the values that appear in Figure 3.

3. Eddy losses

In case the magnetic flux lines pass through a conducting material, eddy currents develop "eddy losses" [11–13]. In our implementation, explained in section 4, this happens in the aluminium plate, which is conducting. To explain the modifications to the equivalent circuit in Figure 3, due to eddy losses we will use the canonical transformed configuration in Figures 1 or 2, assuming the core specific conductivity is σ. For simplicity let us assume the core cross section has a circular shape of radius a, as in Figure 4. The zero order magnetic field, which is uniform in the z direction in

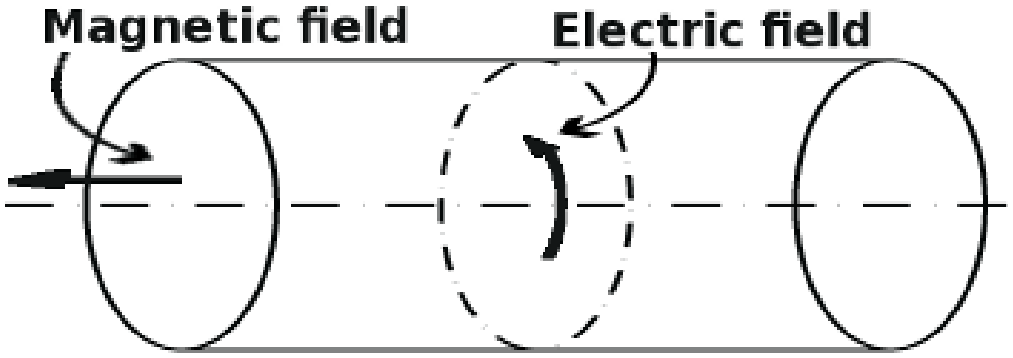

Figure 4. Circular cross section core of specific conductivity σ, and radius a. The zero order magnetic field creates the first order circular electric field, giving rise to a circular current. The first order circular current creates a second order z directed magnetic field.

cylindrical coordinates, creates the first order circular electric field at distance r from the cylinder centre, as follows:

$$2\pi r E_{\varphi}^{(1)} = -\frac{d}{dt}\left[\Phi\frac{\pi r^2}{\pi a^2}\right] = -j\omega\Phi\frac{r^2}{a^2} \Rightarrow E_{\varphi}^{(1)} = -j\omega\Phi\frac{r}{2\pi a^2} \Rightarrow J_{\varphi}^{(1)} = \sigma E_{\varphi}^{(1)} \qquad (12)$$

where $E_{\varphi}^{(1)}$ is the first order circular electric field, Φ is the zero order magnetic flux and $J_{\varphi}^{(1)}$ is the first order circular current density called eddy current. From Ampere law one gets the second order magnetic field

$$H_z^{(2)} = \int_r^a dr' \left[J_{\varphi}^{(1)}(r') + j\omega\epsilon E_{\varphi}^{(1)}(r')\right] = \int_r^a dr'(\sigma + j\omega\epsilon)E_{\varphi}^{(1)}(r'), \qquad (13)$$

where $\epsilon = \epsilon_0\epsilon_r$. However, $\sigma \gg \omega\epsilon$, so that one may safely ignore the displacement current term, obtaining

$$H_z^{(2)} = \int_r^a dr' J_{\varphi}^{(1)}(r') = -\frac{j\omega\sigma}{4\pi}\Phi\left[1 - \left(\frac{r}{a}\right)^2\right] \qquad (14)$$

from which one obtains the second order magnetic flux

$$\Phi^{(2)} = 2\pi\mu\int_0^a r dr H_z^{(2)}(r) = -\frac{j\omega\sigma\mu a^2}{8}\Phi, \qquad (15)$$

so that the total magnetic flux is

$$\Phi_{Total} = \Phi + \Phi^{(2)} = \Phi \left[1 - \frac{j\omega\sigma\mu a^2}{8} \right]. \tag{16}$$

The voltage induced by this total flux on an coil with N turns is

$$V = j\omega N \Phi_{Total} = j\omega N\Phi + \frac{\omega^2\sigma\mu a^2}{8} N\Phi, \tag{17}$$

which has an inductive part and a ohmic part as can be seen be setting $N\Phi = LI$:

$$V = j\omega LI + \frac{\omega^2\sigma\mu a^2}{8} LI \equiv j\omega LI + R_{AC} I, \tag{18}$$

and this holds for either the self induced voltage or the mutual induced voltage, so that R_{AC} is proportional to the self or mutual inductance, defining a resistance in series with the self or mutual inductance. Therefore, defining $R_{AC\,1}$, $R_{AC\,2}$ and $R_{AC\,12}$ the resistances associated with L_1, L_2 and M respectively, and naming the copper losses resistances of the coils $R_{DC\,1}$ and $R_{DC\,2}$, one obtains the equivalent circuit in Figure 5. As mentioned before, in the case of strong coupling either $R_{AC\,1} - R_{AC\,12}$

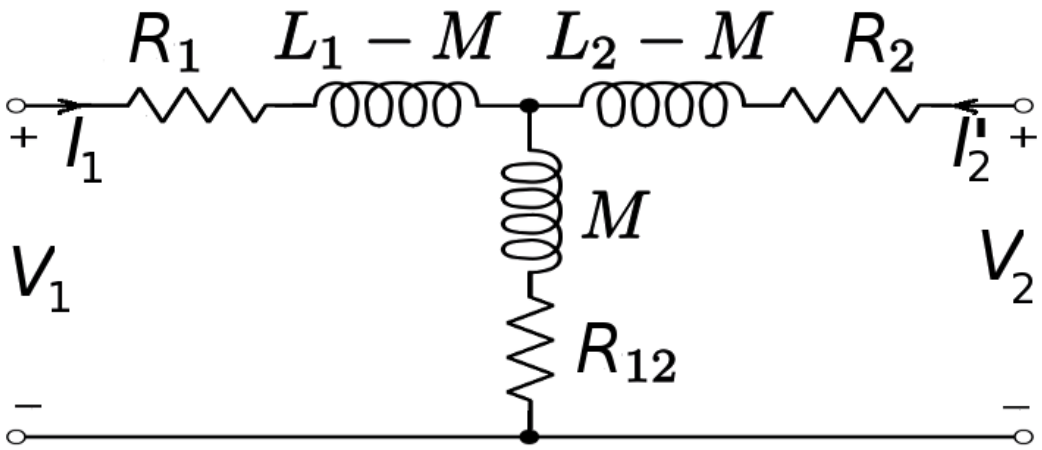

Figure 5. Equivalent circuit for the transformer with losses. In the circuit $R_1 = R_{DC\,1} + R_{AC\,1} - R_{AC\,12}$, $R_2 = R_{DC\,2} + R_{AC\,2} - R_{AC\,12}$ and $R_{12} = R_{AC\,12}$.

or $R_{AC\,2} - R_{AC\,12}$ is negative, but this is no problem, because the overall AC (eddy) losses are positive. For transformers built on a core [11–13], one reflects the voltages and currents to the primary, by scaling them according to N_1/N_2 and N_2/N_1 respectively, in which case the values $R_{AC\,1} - R_{AC\,12}$ and $R_{AC\,2} - R_{AC\,12}$ vanish (in case of strong coupling), remaining only with the $R_{AC\,12} = R_{12}$ in series with M, which becomes in this case the core inductance as seen from the primary L_1. Usually, this R_{12} resistance in series with M is recalculate as a parallel resistance named R_{core}. So for a strong coupling the circuit in Figure 5 reduces correctly to the "regular" equivalent circuit of a transformer.

4. Charging System implementation

We implemented the pacemaker charging system using the ANSYS "Maxwell" and "Simplorer" tools. We used the ANSYS human body model as the medium between the primary and secondary coils, where the primary coil is outside the body, and the secondary coil is inside the human body, as shown in Figure 6. The detailed

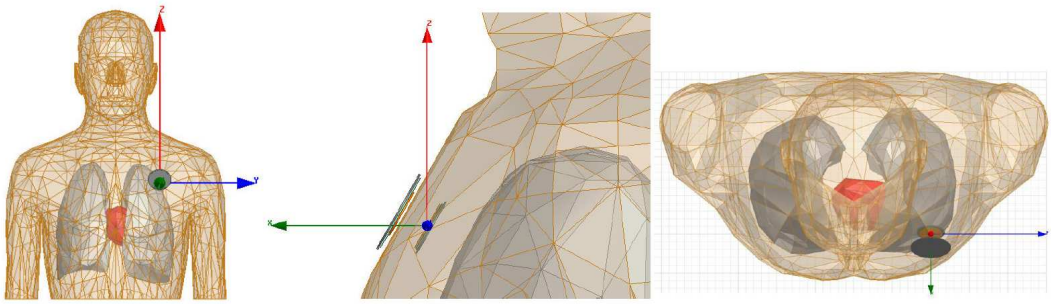

Figure 6. The pacemaker charging system analysed in the ANSYS human body model. The primary coil is outside the body, and the secondary coil is inside the human body.

implementation of the charging system is shown in Figure 7. From our inquiry at

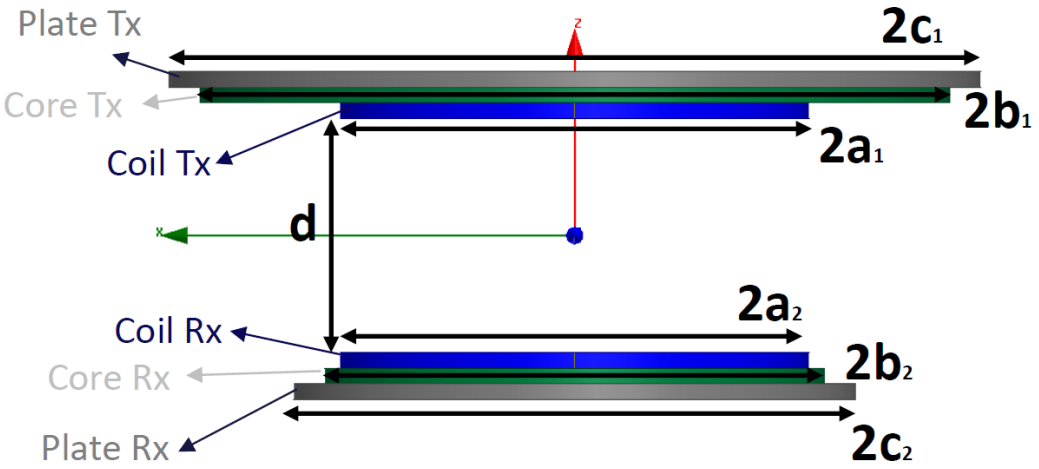

Figure 7. Implementation of the pacemaker charging system. "Tx" and "Rx" represent the primary and secondary sides of the transformer. Both coil have 10 turns and radii $a_1 = a_2 = 15$ mm. Beside each coil we use ferrite core plates of $\mu_r = 2400$ having radii $b_1 = 24$ mm and $b_2 = 16$ mm for primary and secondary, respectively. Next to the ferrite cores we use aluminium plates of conductivity $\sigma = 3.8e7$ S/m, having radii $c_1 = 26$ mm and $c_2 = 18$ mm for primary and secondary, respectively. The thickness of the coils, ferrite and aluminium plates is 1mm. The distance between primary and secondary has been chosen $d = 15$mm.

hospitals, it comes out that pacemakers are implanted beneath the collarbone, where a small pocket for the device is created, and this is at most 15mm below the skin level, this is the reason for our choice $d = 15$mm. Being separated in space, the primary and secondary fluxes cannot coincide on the same trajectories, so that the coupling coefficient would be very small without the above additional ferrite cores and aluminium plates. The contribution of the ferrite and aluminium is shown in Figure 8. In Figure 9 we show the "Maxwell" simulated configuration for obtaining the equivalent circuit components. The analysis has been done at the frequency of 20kHz,

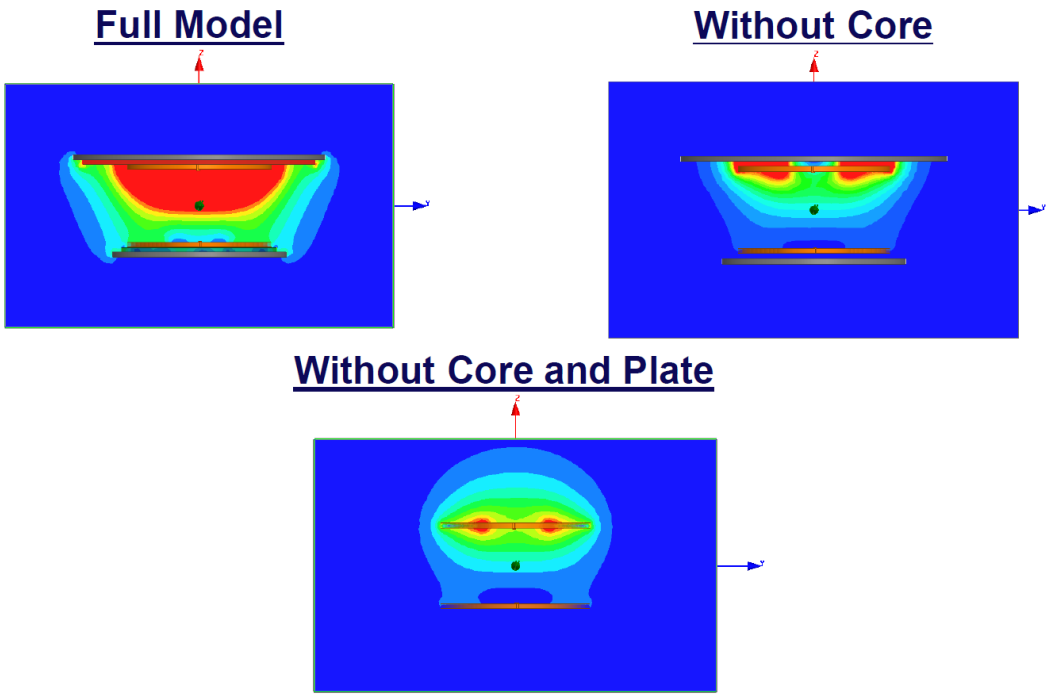

Figure 8. Magnetic field in case the primary is fed: warmer colours represent higher magnetic fields. Without the ferrite and the aluminium, the primary field is symmetric around the primary coil, while we need it directed toward the secondary coil. With the aluminium only, the primary magnetic field is directed toward the secondary, but still weak. The core strengthen this field significantly, as can be seen in the "Full model" plot. It is to be mentioned that the aluminium and the ferrite plates substantially increase the coupling coefficient, which is critical for obtaining an efficient system.

and the equivalent circuit results from the "Maxwell" simulation are: $L_1 = 4168.5$ nH,

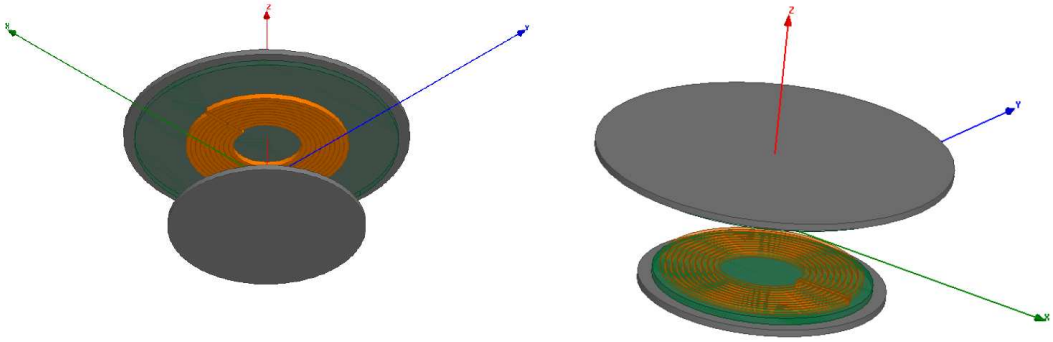

Figure 9. The "Maxwell" tool simulated configuration for the primary and secondary coils for obtaining the equivalent circuit components.

$L_2 = 3700.2$ nH, $M = 522.69$nH, $R_1 = 18.78$mΩ, $R_2 = 21.89$mΩ and $R_{12} = 1.78$mΩ (see Figure 5). The coupling coefficient is 0.133 according to Eq. 4.

For comparison, we also checked the result of this simulation without the human body model and we obtained a coupling coefficient bigger by only 15%. This means that the effect of the human body is moderate to low at the frequency of 20kHz we use, due to the low human body electric conductivity at this frequency and due to the fact that the human body has no magnetic properties.

To obtain a good power transfer, we added matching networks consisting of a ca-

pacitor and an inductor at each side, and activated the "Simplorer" to optimize the configuration for the best transmission coefficient s_{12} of the scattering matrix S, [14–16] defined for a characteristic impedance of 50Ω. Clearly, without losses one would arrive to $s_{12} = 1$, or 0dB, but suffering from losses, we arrive to a lower value 0.72 or -2.86dB. In Figure 10 we show the 'Simplorer" circuit with the optimized matching networks. The small block in the figure represents the transformer block, analysed by "Maxwell", as shown in Figure 9, which basically can be represented by an equivalent circuit as shown in Figure 5. It is to be mentioned that for any non zero coupling coeffi-

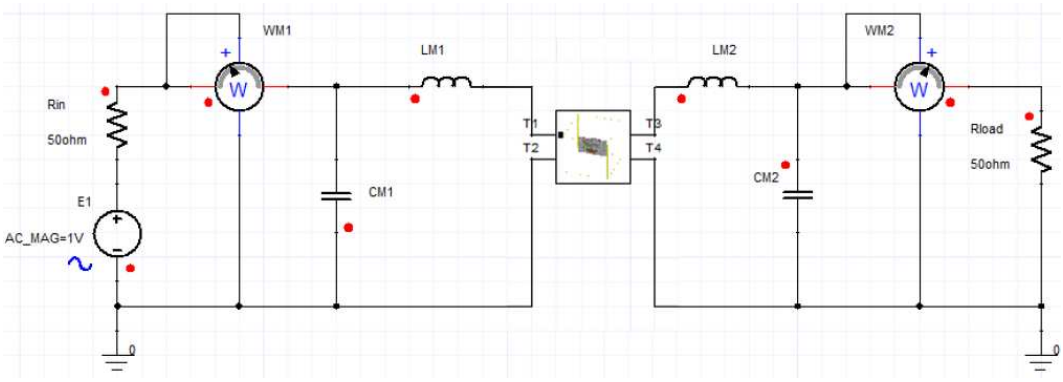

Figure 10. The "Simplorer" circuit with matching networks at both sides. The block with entry port T_1, T_2 and exit port T_3, T_4 represents the transformer block, analysed by "Maxwell", as shown in Figure 9. The watt-meters measure input and output power, to optimize the matching networks. The values obtained for the components of the matching networks are: $C_{M1} = 4.45\mu$F, $C_{M2} = 4.13\mu$F, $L_{M1} = 10.09\mu$H and $L_{M2} = 11.66\mu$H.

cient, one may find matching network components to get a high value of s_{12}, i.e. a good transfer. However, as lower the coupling coefficient is, the matching components get more unrealistic and eccentric values which cannot be used in a real implementation. The values that we got are quite moderate and implementable.

For the circuit in Figure 10, the "Simplorer" calculated the performances of the system, described by the S parameters [16], namely the transmission coefficient s_{12}, which is highest at the centre frequency, and the reflection coefficient (return loss) s_{11}, which is lowest at the centre frequency. The absolute value of the S parameters are shown in dB in Figure 11. At the centre frequency, the transmission coefficient is -2.86dB, or 0.72, so that our system has an efficiency of 72%.

From the circuit in Figure 10, one may easily confirm the results shown in Figure 11 by cascading 5 ABCD matrices to obtain the ABCD matrix of the whole circuit, from which one obtains the S parameters [16, 17], using

$$s_{12} = 2/[A + B/R + RC + D] \tag{19}$$

$$s_{11} = -0.5 s_{12}[A - B/R + RC - D] \tag{20}$$

where $R = 50\Omega$ is the characteristic impedance for which the S parameters have been defined. Figure 12 illustrates the matching process on the Smith chart. Because jumps between points which differ by the real *and* imaginary parts of the impedance are difficult to follow on a Smith chart, we neglected the losses, i.e. used for the transformer block in Figure 10 only the components which appear in Figure 3. After adding L_{M2} to $L_2 - M$, and L_{M1} to $L_1 - M$, we get a "Y" network with branches $L_2 - M + L_{M2}$,

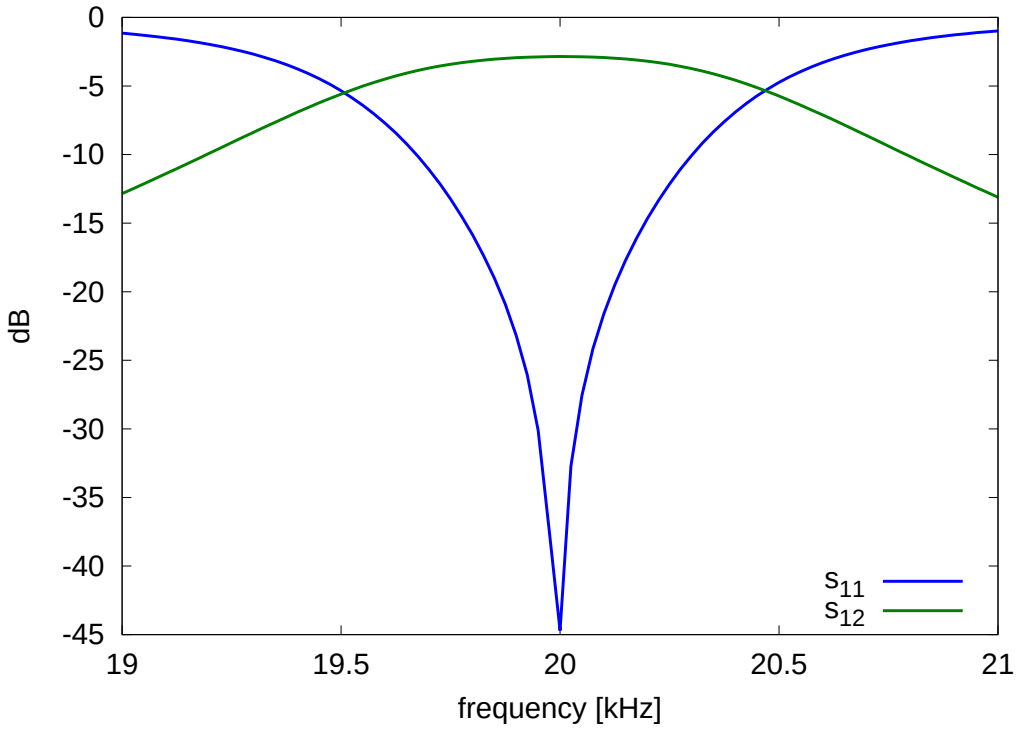

Figure 11. The absolute values of the S parameters, expressed in dB, computed by the "Simplorer".

$L_1 - M + L_{M1}$ and M, which is transformed into "Δ" network, obtaining a "Π" network having an inductor in parallel with a capacitor at each side and an inductor in between as shown in Figure 12. The impedance of those components at centre frequency 20kHz, normalized by the characteristic impedance 50Ω are shown in the figure. Clearly, because the matching components have been optimized for the lossy network, the matching on the Smith does not come out perfect, so that s_{11} comes out bigger than in Figure 11, but still small. We start with a matched load at the right end, i.e. 1 on the chart and add the admittance of the right LC circuit $1/(-1.037j) = 0.96j$, going on the green line to the point $1 + 0.96j$. To represent impedance we go on the red line to the opposite point $0.52 - 0.5j$. Here we add the middle inductor $1.052j$ going on the blue line to $0.52 + 0.552j$, and because the next step is to add in parallel we move to the admittance at the opposite side at $0.904 - 0.963j$ on the purple line. Finally we add the admittance of the left LC circuit $1/(-1.03j) = 0.971j$ going on the black line to $0.904 + 0.008j \simeq 0.904$. Ideally, if we would have taken the full model with losses, we should have arrived much closer to 1. The value of s_{11} obtained from the Smith chart is $|(0.904 - 1)/(0.904 + 1)| = 0.05$, or -25.9dB, instead of the exact value of -44.7dB obtained in Figure 11 with the full model.

5. Conclusions

This work explains the principles of wireless power transfer by mutual inductance and shows the design of a pacemaker charging system done with ANSYS "Maxwell" and "Simplorer" tools. The pacemaker charging system is limited to small dimensions (especially the side in the body), as shown in Figures 6 and 7, and the distance between

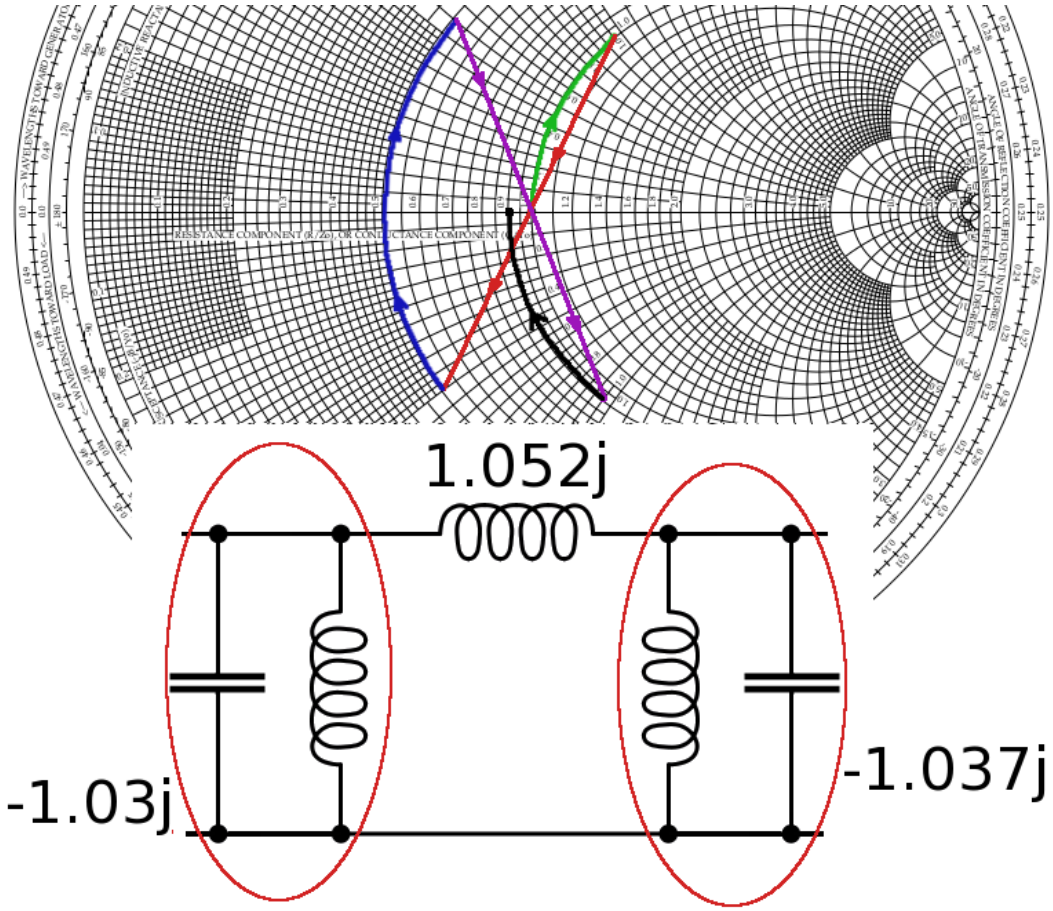

Figure 12. The matching process on the Smith chart.

primary and secondary coils cannot be much smaller than their radii. In spite of those obstacles, by using the aluminium plates to direct the magnetic flux, and the ferrite plates to strengthen it, we obtained a good coupling coefficient of 0.133, allowing the design of implementable matching networks to achieve a good system efficiency of 72%.

We intend to generalize this design to include wireless data transmission from an implanted antenna [18] together with the charging system presented here. The implanted charging system and antenna may mutually influence each other, hence a redesign of both is necessary.

References

[1] Mallela VS., Ilankumaran V. and Rao NS., "Trends in Cardiac Pacemaker Batteries", Indian Pacing and Electrophysiology Journal 4(4):201 (2004)

[2] Maisel W.H. et al. "Pacemaker and ICD generator malfunctions: analysis of Food and Drug Administration annual reports", JAMA 295(16), 295:1901 (2006)

[3] Song K. et. al., "Subdermal Flexible Solar Cell Arrays for Powering Medical Electronic Implants", Adv. Healthc. Mater., doi: 10.1002/adhm.201600222 (2016)

[4] Campi T., Cruciani S., Palandrani F., De Santis V. , Hirata A. and Feliziani M., "Wireless Power Transfer Charging System", IEEE Trans. Microw. Theory Tech. 64(2), pp 633-642

(2016)
[5] Campi T., Cruciani S., De Santis V. and Feliziani M., "EMF Safety and Thermal Aspects in a Pacemaker Equipped With a Wireless Power Transfer System Working at Low Frequency", IEEE Trans. Microw. Theory Tech. 64(2), pp 375-382 (2016)
[6] Ahmad Q.S., Chandel T.A. and Ahmad S., "Wireless Power Transmission to Charge Pacemaker Battery", National conference on "Challenges opportunities for technological innovation in India" (cotii -2015), Ambalika Institute of Management Technology, Lucknow, India, (February 2015)
[7] Xiong Q., "Wireless Charging Device for Artificial Cardiac Pacemaker", International Conference on Information Technology and Management Innovation (ICITMI), Shenzhen, China, (September 2015)
[8] Chen X.L. , Umenei A.E., Baarman D.W., Chavannes N., De Santis V., Mosig J.R. and Kuster N., "Human Exposure to Close-Range Resonant Wireless Power Transfer Systems as a Function of Design Parameters", IEEE Trans. Electromagn. Compat., 56(5), pp 1027-1034(2014)
[9] Electromagnetic Compatibility and Radio Spectrum Matters (ERM); Radio Equipment in the Frequency Range 9 kHz to 315 kHz for Ultra Low Power Active Medical Implants (ULP-AMI) and Accessories. Part 1: Technical Characteristics and Test Methods, ETSI EN 302 195-1, 2004.
[10] Electromagnetic Compatibility and Radio Spectrum Matters (ERM); Radio Equipment in the Frequency Range 9 kHz to 315 kHz for Ultra Low Power Active Medical Implants (ULP-AMI) and Accessories. Part 2: Harmonized EN Covering Essential Requirements of Article 3.2 of the R&TTE Directive, ETSI EN 302 195-2, 2004.
[11] Chapman S. J., "Electric Machinery Fundamentals", 4th edition, McGraw-Hill (2005)
[12] McPherson G. and Laramore R.D., "An Introduction to Electrical Machines and Transformers", John Wily & Sons, 1991.
[13] Del Toro, "Electrical Machines and Power Systems" , Prentice-Hall, 1990.
[14] Waters B.H., Sample A.P. and Smith J.R., "Adaptive Impedance Matching for Magnetically Coupled Resonators", PIERS Proceedings, Moscow, Russia, August 1923 (2012)
[15] Bito J., Jeong S. and Tentzeris M.M., "A Real-Time Electrically Controlled Active Matching Circuit Utilizing Genetic Algorithms for Wireless Power Transfer to Biomedical Implants", IEEE Transactions on Microwaves, 64(2), 365:374 (2016)
[16] Pozar D. M., "Microwave Engineering", Wiley India Pvt., 2009
[17] Vulfin V. and Ianconescu R., "Transmission of the maximum number of signals through a Multi-Conductor transmission line without crosstalk or return loss: theory and simulation", IET MICROW ANTENNA P, 9(13), pp. 1444-1452 (2015)
[18] Shimonov N., Vulfin V., Sayfan-Altman S. and Ianconescu R., "Design of an implanted antenna inside the human body for a pacemaker application", ICSEE International Conference on the Science of Electrical Engineering, Eilat, Israel, November 16-18 (2016)